Pergamon

Int. J. Heat Mass Transfer. Vol. 39, No. 14, pp. 3057–3066, 1996

0017-9310/96 $15.00 + 0.00

0017-9310(95)00330-4

Numerical and experimental studies of three-dimensional plate-fin and tube heat exchangers

JIIN-YUH JANG and MU-CHENG WU

Department of Mechanical Engineering, National Cheng-Kung University, Taiwan, Taiwan 701, Republic of China

and

WEN-JENG CHANG

Department of Mechanical Engineering, Feng-Chia University, Taichung, Taiwan 400, Republic of China

(*Received* 16 *July* 1995)

Abstract—Fluid flow and heat transfer over a multi-row (1–6 rows) plate-fin and tube heat exchanger are studied numerically and experimentally. Fluid flow is incompressible, three-dimensional and laminar. The effects of different geometrical parameters such as tube arrangement, tube row numbers and fin pitch (8–12 fins per inch) are investigated in detail for the Reynolds number (based on the fin spacing and the frontal velocity) ranging from 60 to 900. The average heat transfer coefficient of staggered arrangement is 15%–27% higher than that of in-lined arrangement, while the pressure drop of staggered configuration is 20%–25% higher than that of in-lined configuration. Average Nusselt number is decreased as the number of tune row is increased from 1 to 6. The number of tube row has a small effect on the average heat transfer coefficient as the row numbers became greater than 4. The numerical results for the average heat transfer coefficient and pressure drop agree well with the experimental measurements. Copyright © 1996 Elsevier Science Ltd.

1. INTRODUCTION

Plate-fin and tube heat exchangers are employed in a wide variety of engineering applications, for instance, in air conditioning units, process gas heaters and coolers, compressor intercoolers and aftercoolers, etc. A bank of tubes shares common fins, as shown in Fig. 1. Generally, a liquid flows through the tubes and a gas flows through the channels formed by the neighboring fins, around the tube bank. The heat transfer between the gas and the fins and tube surfaces is determined by the flow structure which is three-dimensional (3D). The flow can be treated as laminar since the characteristic Reynolds number based on the average velocity and the hydraulic diameter of the channel will be less than 2000.

There have been a number of studies on the pressure drop and heat transfer characteristics of bare tube banks in cross flow. Most of the earlier studies were experimental in nature, and an excellent review is given in Zukauskas [1]. For 2D numerical simulations, Thom and Apelt [2] used the conformal mapping technique to solve the flow past a bare tube bundle. Le Feuvre [3] employed nonuniform Cartesian grids to obtain a numerical solution for an in-line tube bank with uniform tube wall temperature. Launder and Massey [4] and Fujii *et al.* [5] used the hybrid polar-Cartesian grid system for a staggered and an in-line tube bank, respectively. Wung and Chen [6, 7] employed the boundary-fitted coordinate system to study the flow field and heat transfer for both staggered and in-lined tube arrays. Kundu *et al.* [8–10] numerically and experimentally studied the pressure and heat transfer in cross flow over cylinders between two parallel plates. It is noted that 2D flow fields cannot predict heat transfer between the fluid and the fin, hence their simulations have limited application.

Available experimental information on the plate-fin and tube heat exchangers have been presented, reviewed and correlated in the open literatures. Saboya and Sparrow [11–13] used the naphthalene mass transfer method to measure the local coefficients for one-row, two-row and three-row plate-fin and tube heat exchangers. Rich [14, 15] investigated the effects of fin-pitch and number of tube row for staggered plate-fin and tube heat exchangers. Correlations to predict the Colburn (j) and friction factor (f) vs Reynolds number for plain fins on staggered tubes were developed by McQuiston [16] and Gray and Webb [17]. The experimental data available up to 1994 have been reviewed in the book by McQuiston and Parker [18].

Owing to the complicated 3D flow between fins, the numerical studies are very difficult. For convenience

NOMENCLATURE

C_p	pressure coefficient, $(p-p_{in})/(\frac{1}{2}\rho w_{in}^2)$
h	heat transfer coefficient [W m^{-2}°C^{-1}]
$\bar{h}$	average heat transfer coefficient [W m^{-2}°C^{-1}]
H	fin spacing [mm]
ix	grid number of x-direction
iy	grid number of y-direction
iz	grid number of z-direction
k	thermal conductivity [W m^{-1}K^{-1}]
n	dimensionless unit normal vector
Nu	local Nusselt number, $h \cdot H/k$
$\overline{Nu}$	average Nusselt number
p	pressure [Pa]
P	dimensionless pressure, $p/(\rho w_{in}^2)$
Pr	Prandtl number, v/α
q''	heat flux [W/m^{-2}]
Re_H	Reynolds number, $h \cdot H/v$
T	temperature [°C]
T_b	bulk mean temperature
T_{in}	inlet temperature [°C]
T_w	wall temperature [°C]
U_i, U_j	dimensionless velocity vectors
w_{in}	frontal velocity [m s^{-1}]
x	x-direction coordinate
X	dimensionless x-direction coordinates, x/H.

Greek symbols

α	thermal diffusivity, [m^2 s^{-1}]
ρ	density of fluid [kg m^{-3}]
v	kinematic viscosity [m^2 s^{-1}]
θ	circumferential angle
Θ	dimensionless temperature, $(T-T_w)/(T_{in}-T_w)$
Θ_b	dimensionless bulk mean temperature, $(T_b-T_w)/(T_{in}-T_w)$.

Subscripts

w	solid surface.

of calculation, Yamashita *et al.* [19, 20] used a fundamental model, consisting of a pair of parallel plates and a square cylinder passing perpendicularly through the plates, which simulate plate-fins and a tube. Bastani *et al.* [21] employed one circular tube as the computation domain and assumed that the flow was fully developed with periodic boundary condition to simulate the heat and flow field of in-lined tube arrays. Recently, 3D laminar and turbulent heat transfer around tube banks are presented by Zdravistch *et al.* [22], who used the Dirchlet and Neumann boundary conditions at the inlet and outlet boundaries, respectively, for each computational element. The calculated outlet values are used as inlet boundary conditions for the next computational element deeper into the tube bank. All of the works mentioned above can not satisfy either the realistic geometry or the inlet–outlet conditions for an actual plate-fin and tube heat exchanger. This has motivated the present investigation. The present study provides the numerical solutions for the actual multi-row (1–6 rows) plate-fin and tube heat exchangers. Therefore, a whole computational domain (1–6 rows) from the fluid inlet to outlet is solved directly. In addition, the numerical results for four row plate-fin and tube heat exchangers in staggered arrangement with three different fin pitches (8, 10, 12 fins/in) under different values of inlet frontal velocity are compared with those obtained from the experiments conducted in a steady-state open induced wind tunnel.

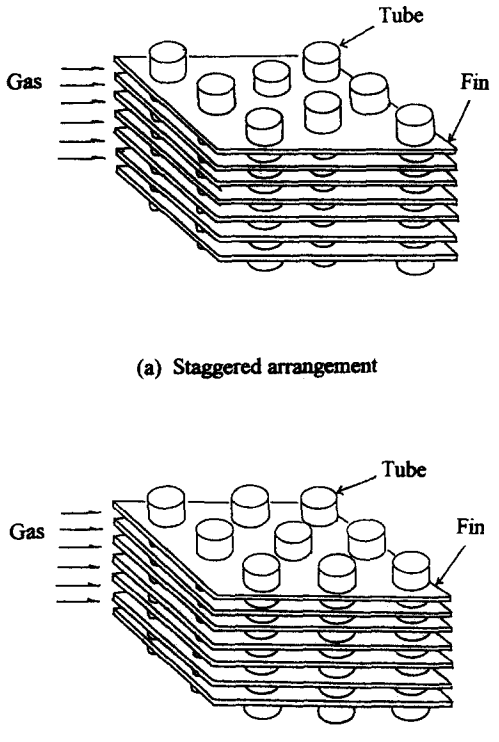

(a) Staggered arrangement

(b) In-lined arrangement

Fig. 1. Schematic of a plate-fin tube heat exchanger.

2. MATHEMATICAL ANALYSIS

2.1. *Governing equations*

The dashed lines in Fig. 2 designate the computational domain. Assuming symmetry conditions on the mid-plane between two fins, the bottom and

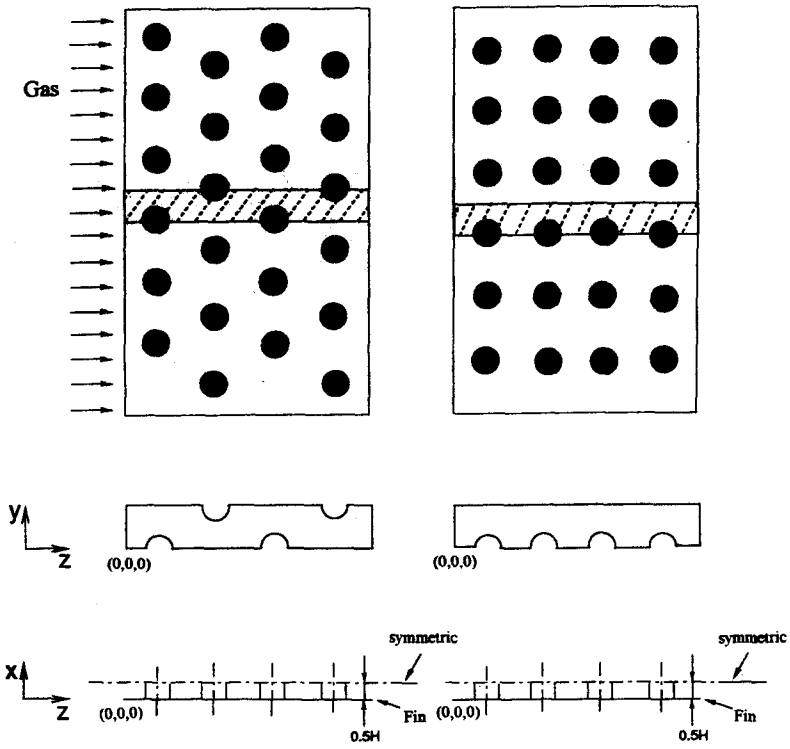

(a) Staggered (b) In-lined

Fig. 2. The computation domain and coordinate system.

top boundaries simulate the fin and the mid-plane, respectively. The coordinate system is also illustrated in the figure. The fluid is considered incompressible with constant properties and the flow is assumed to be laminar, steady, 3D and exhibiting no viscous dissipation. The dimensionless equations for continuity, momentum and energy may be expressed in tensor form as

$$\frac{\partial U_i}{\partial X_i} = 0$$

$$\frac{\partial}{\partial X_j}(U_i U_j) = -\frac{\partial P}{\partial X_i} + \frac{1}{Re_H}[\nabla^2 U_i]$$

$$\frac{\partial}{\partial X_j}(\Theta U_j) = \frac{1}{Re_H Pr}[\nabla^2 \Theta].$$

In the above equations, the velocity has been non-dimensionalized with the uniform inlet frontal velocity w_{in} at the channel inlet, all length coordinates with the channel height (fin spacing) H, and the pressure with ρw_{in}^2. The dimensionless temperature is defined as $\Theta = (T - T_w)/(T_{in} - T_w)$. The Reynolds number is $Re_H = w_{in} \cdot H/\nu$ and Pr is the fluid Prandtl number, which is set to be equal to 0.736 in the present study.

2.2. *Boundary conditions*

Because the governing equations are elliptic in spatial coordinates, the boundary conditions are required for all boundaries of the computation domain. At the upstream boundary, uniform flow with velocity $w_{in}\mathbf{k}$ and temperature T_{in} are assumed. At the downstream end of the computational domain, located seven times the tube diameter from the last downstream row cylinder, streamwise gradient (Neumann boundary conditions) for all the variables are set to zero. At the symmetry planes normal gradients are set to zero. At the solid surfaces, no-slip conditions and constant wall temperature T_w are specified.

The pressure drop is expressed in terms of the dimensionless pressure coefficient, C_p, defined as

$$C_p = \frac{p - p_{in}}{\frac{1}{2}\rho w_{in}^2}$$

where p_{in} is the pressure at inlet.

The local heat transfer coefficient h is defined as

$$h = \frac{q''}{T_w - T_b}$$

where q'' is the local heat flux and T_b is the local bulk mean temperature of the fluid. The local heat transfer coefficient can be expressed in the dimensionless form by the Nusselt number Nu, defined as

$$Nu = \frac{h \cdot H}{k} = \left.\frac{\partial\left(\frac{\Theta}{\Theta_b}\right)}{\partial n}\right|_{wall}$$

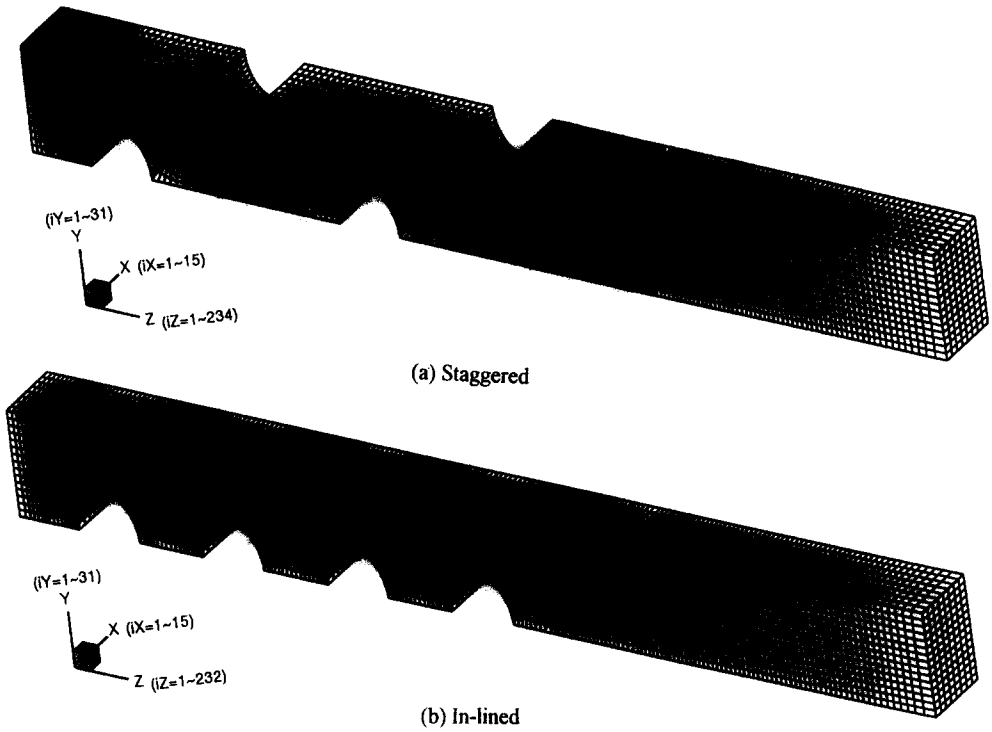

Fig. 3. Computation grid system.

where $\Theta_b = (T_b - T_w)/(T_{in} - T_w)$ is the local dimensionless bulk mean temperature; n is the dimensionless unit vector normal to the wall. The average Nusselt number $\overline{Nu}$ then can be obtained by

$$\overline{Nu} = \frac{\int Nu \, dA_s}{\int dA_s}$$

where dA_s is the infinitesimal area of the wall surface.

3. NUMERICAL METHOD

In this study, the boundary-fitted coordinate system was used to generate a general curvilinear coordinate system by numerically solving Laplace equations with proper control of grid densities. The governing equations are solved numerically using a control volume based finite difference formulation. The SIMPLER algorithm [23] is used to solve iteratively the system of finite-difference equations. The hybrid scheme is employed for the treatment of convection and diffusion terms. A grid system of $15 \times 31 \times 234$ grid points is adopted typically in the computation domain for a four tube row arrangement as shown in Fig. 3. However, a careful check for the grid independence of the numerical solutions has been made to ensure the accuracy and validity of the numerical results. For this purpose, three grid systems, $11 \times 26 \times 194$, $15 \times 31 \times 234$ and $17 \times 33 \times 261$, are tested. It is found that for $Re_H = 400$, the relative errors in the local and averaged Nusselt numbers between the solutions of $15 \times 31 \times 234$ and $17 \times 33 \times 261$ are less than 4%. Computations were performed on VAX9420. Typical CPU times are 15 h for each case.

4. TEST SECTIONS AND EXPERIMENTAL APPARATUS

Three heat exchangers of flat fin geometry and in staggered configuration with four rows and three different fin pitches were tested in the present study. Their detailed geometrical parameters are tabulated in Table 1. Experiments were conducted in an induced draft wind tunnel as shown in Fig. 4. The air flow is driven by a 3.73 kW (5h.p.) centrifugal fan with an

Table 1. Geometrical parameters of the test sections

Test Section	1	2	3
Tube o.d. [mm]	15.9	15.9	15.9
Tube thickness [mm]	1.05	1.05	1.05
Length [mm]	400	400	400
Width [mm]	132	132	132
Height [mm]	247	247	247
Fin thickness [mm]	0.25	0.25	0.25
Fin pitch [fins in]	8	10	12
Xt [mm]	33	33	33
Xl [mm]	38	38	38
Tube number	24	24	24
Row number	4	4	4
Pass number	4	4	4

Note: (1) Xt: transverse tube spacing; (2) Xl: longitudinal tube spacing; (3) tube material: copper; (4) fin material: aluminum.

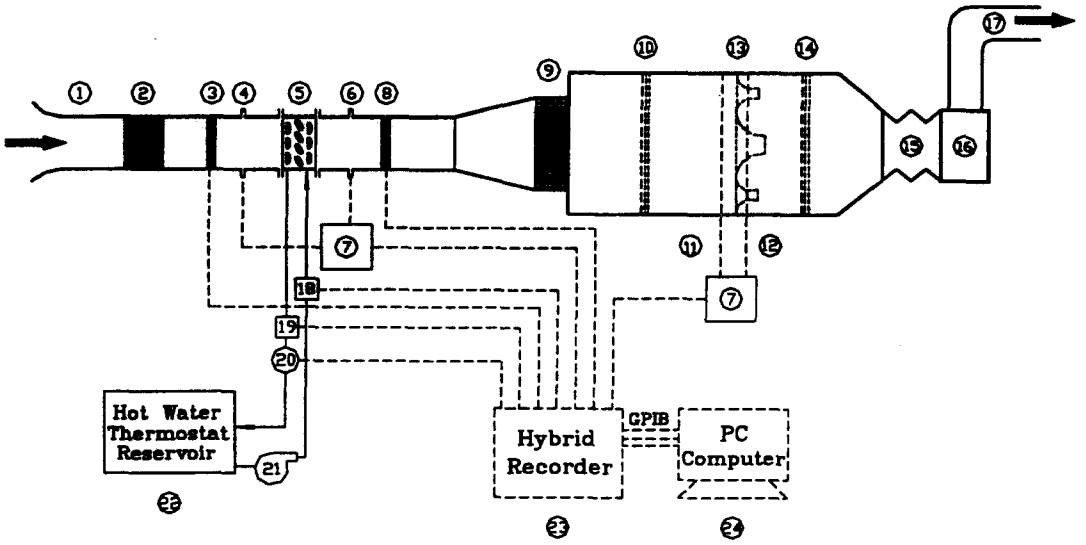

Fig. 4. Schematic diagram of the experimental setup: (1) inlet, (2) air straightener, (3) air side inlet temperature measuring station, (4) pressure tap (inlet), (5) test section, (6) pressure tap (outlet), (7) differential pressure transducer, (8) air side outlet temperature measuring station, (9) air mixer, (10) air straightener, (11) nozzle pressure tap (inlet), (12) nozzle pressure tap (outlet), (13) multiple nozzle plate, (14) air straightener, (15) flexible duct, (16) variable exhaust fan system, (17) discharge, (18) tube side inlet temperature measuring station, (19) tube side outlet temperature measuring station, (20) volumetric flow meter, (21) pump.

inverter. To avoid and minimize the effect of flow maldistribution in the experiments, an air straightener–equalizer and a mixer are provided. The inlet and the exit temperature across the test section are measured by two T-type thermocouple meshes. The data signals are individually recorded and then averaged. During the isothermal test, the variance of these thermocouples were within ± 0.2°C. In addition, all the thermocouples were pre-calibrated by a quartz thermometer with 0.01°C precision. The pressure drop of the test coil is detected by a precision differential pressure transducer, reading to 0.1 Pa. The air flow measuring station is a multiple nozzle code tester based on the ASHRAE 41.2 standard [24].

The working medium in the tube side is hot water. The inlet temperature is controlled by a thermostat reservoir having an adjustable capacity up to 40 kW. Both the inlet and outlet temperatures are measured by two pre-calibrated RTDs (Pt-100 Ω). Their accuracy is within 0.05°C. The water volumetric flow rate is measured by a magnetic volume flow meter with 0.002 l s^{-1} resolution. All the data signals are collected and converted by a data acquisition system (a hybrid recorder). The data acquisition system then transmits the converted signals through GPIB interface to the host computer for further operation. During the experiments, the water inlet temperature is held constant at 60.0 ± 0.1°C. Frontal velocities range from 0.3 to 6.0 m s^{-1}. Generally, the energy balance between air side and tube side is within 2%. To obtain the average heat transfer coefficient from the measured experimental data, the ε–NTU (effectiveness-number of transfer unit) method is applied [25]. The water side resistance is estimated to be less than 10% of the overall resistance. Note that the copper wall resistance is negligible. Therefore, the dominant thermal resistance is always on the air side. This may resolve any concern about the magnitude and accuracy of the water side that is being subtracted from the overall resistance. Uncertainties in the reported experimental values of the average heat transfer coefficient were estimated by the method suggested by Moffat [26]. The uncertainties ranged from 3.3 to 6.2%. The highest uncertainties were associated with lowest Reynolds number.

5. RESULTS AND DISCUSSION

The numerical results for the actual plate-fin and tube heat exchangers with inlet frontal velocity ranging from 2 m s^{-1} ($Re_H = 400$) for the geometry having four-row deep, tube diameter 15.9 mm (5/8 in), fin pitch 8 fins in^{-1} and tube center spacing 38 mm for both staggered and in-lined arrangements are shown in Figs. 5–8. Figures 5 and 6 illustrate the streamline and the isotherm patterns for the staggered and in-lined arrangements on the yz-plane at $X = 0.0357$ (near fin surface) and $X = 0.4643$ (near mid-plane between two fins), respectively. For the staggered array, because of the repeated blockage of the staggered tube bank, there is a smaller recirculation zone behind each tube, while for the in-lined array, the flow separates at the rear portion of a tube and reattaches at the front portion of the following tube to form a larger stationary recirculation region between the two adjacent tubes, resulting in a dead flow zone. It is also

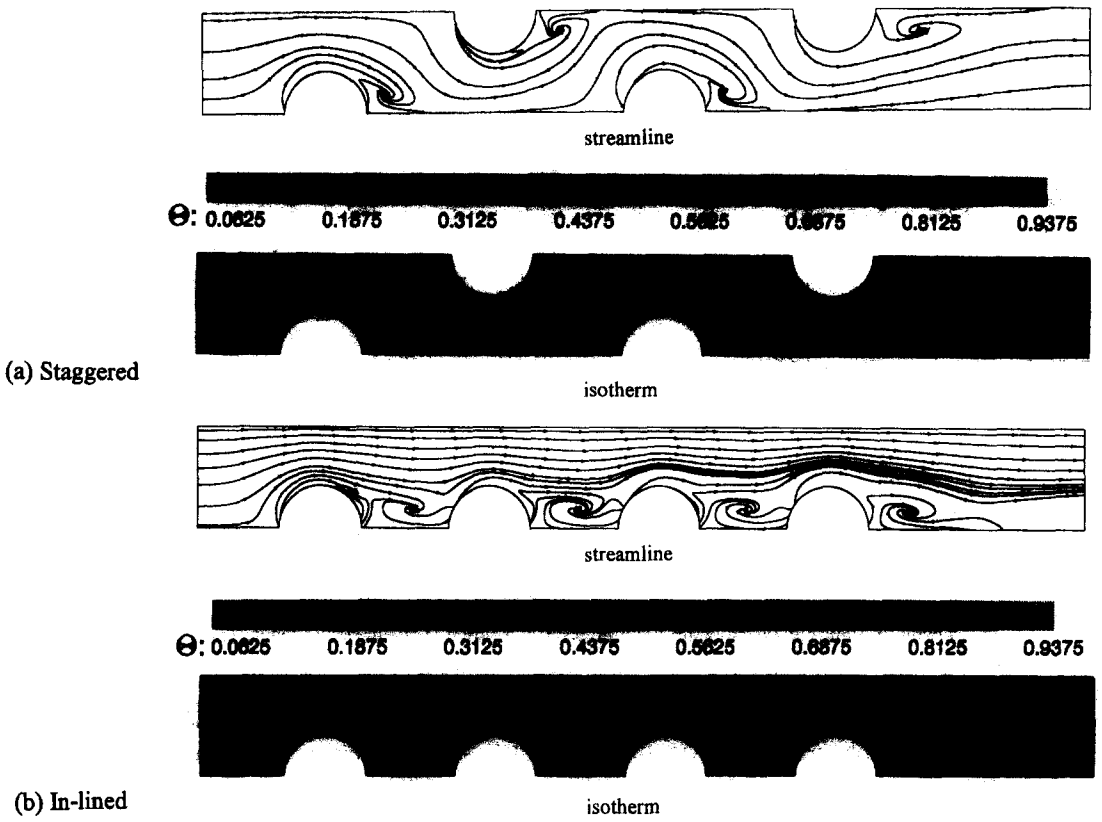

Fig. 5. The streamline and isotherm patterns for the staggered and in-lined arrangements on the yz-plane at $X = 0.0357$ (near the fin surface) for $Re_H = 400$, inlet flow $\Theta = 1$, solid surface $\Theta = 0$.

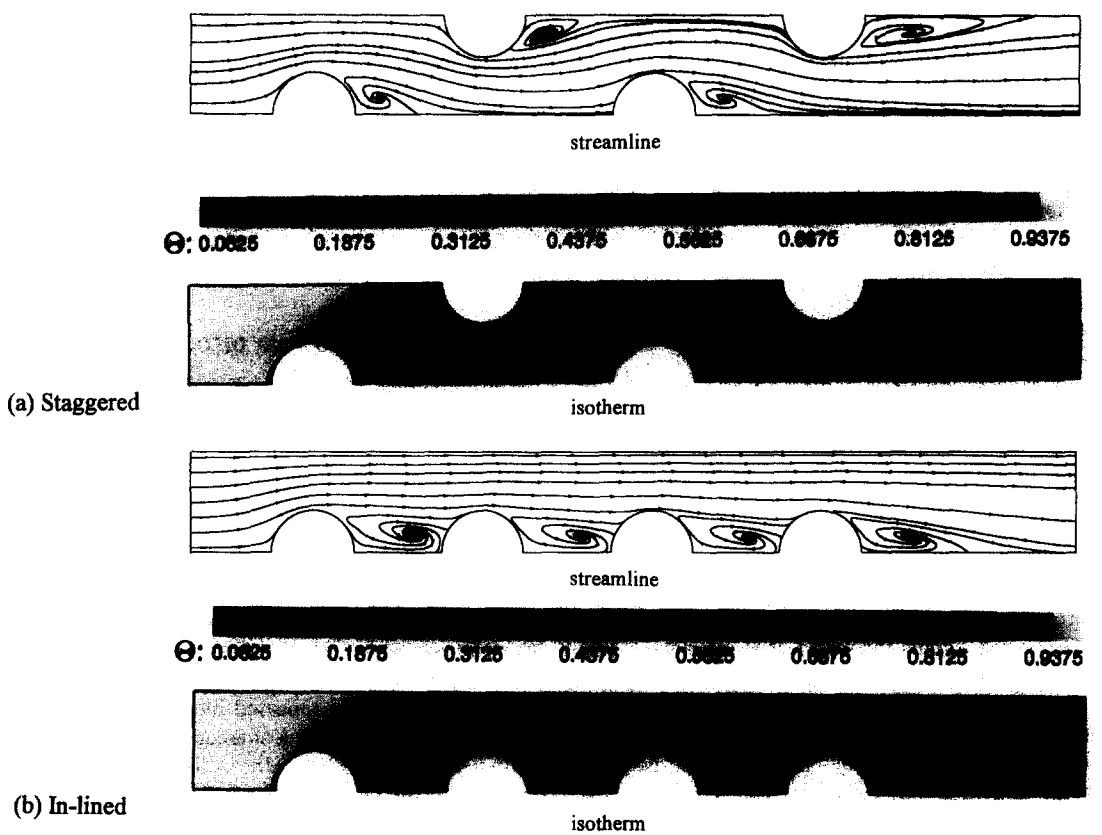

Fig. 6. The streamline and isotherm patterns for the staggered and in-lined arrangements on the yz-plane at $X = 0.4643$ (near the mid-plane) for $Re_H = 400$, inlet flow $\Theta = 1$, solid surface $\Theta = 0$.

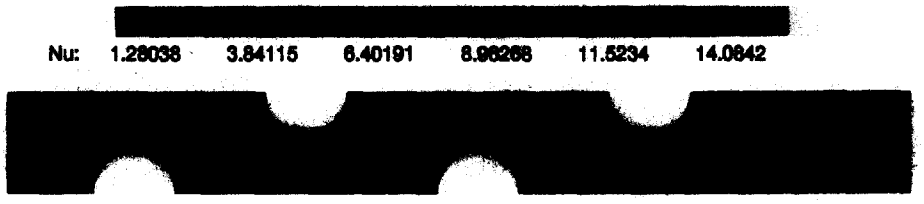

(a) Nusselt number contour for staggered arrangement

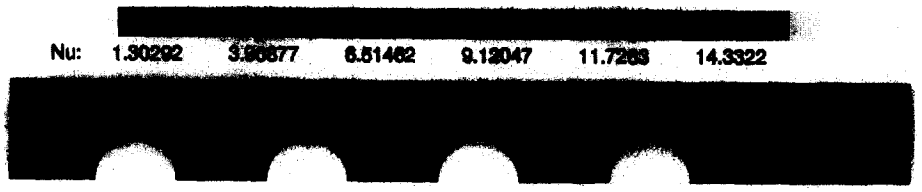

(b) Nusselt number contour for in-lined arrangement

Fig. 7. Nusselt number contours on the fin surface for the staggered and in-lined arrangements for $Re_H = 400$.

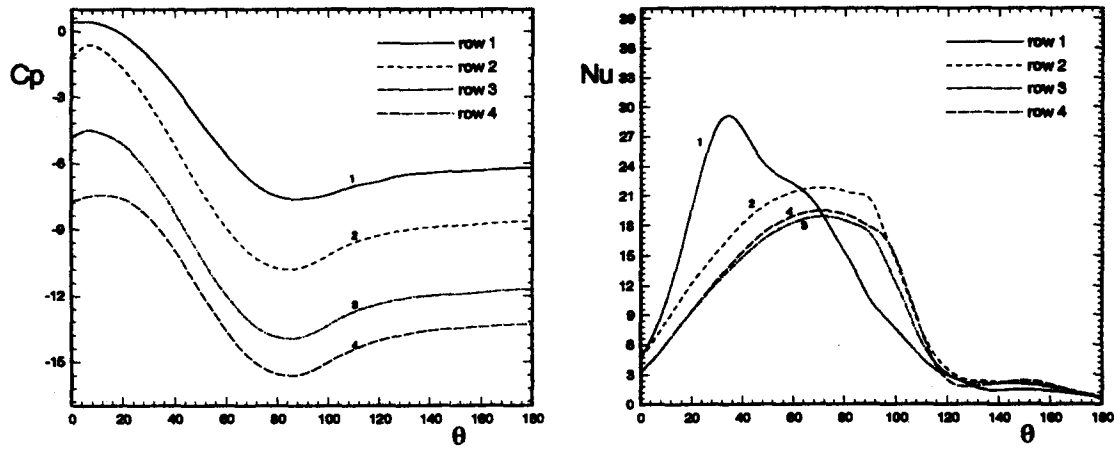

(a) Staggered

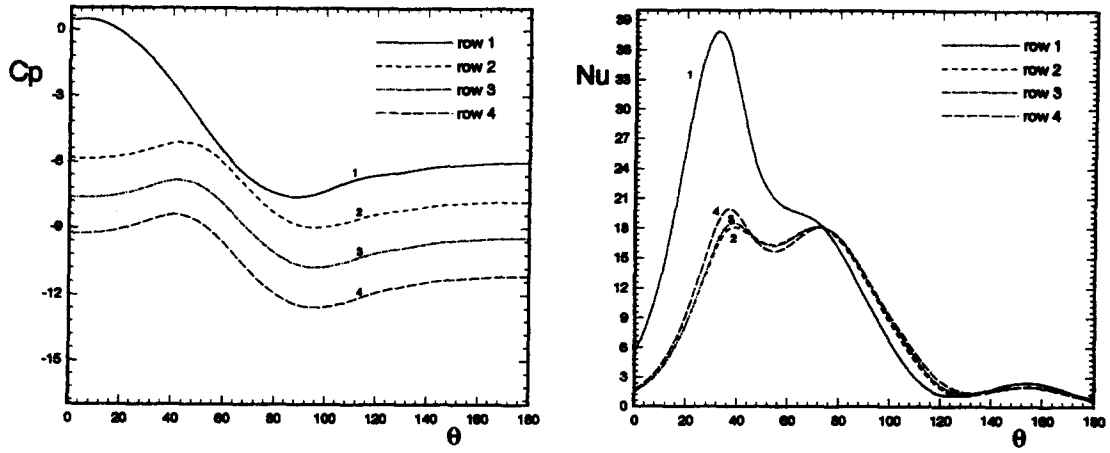

(b) In-lined

Fig. 8. The variations of C_p and Nu around the tube surface at $X = 0.25$, $Re_H = 400$ for the staggered and in-lined arrangements.

seen that the flow pattern and temperature contour on the y–z plane at $X = 0.0357$ and $X = 0.4643$ are quite different. Near the fin surface, there is a backflow zone in front of the tube because of the wall effect, while near the mid-plane, there is no backflow in front of the tube and the flow from upstream approaches the tube just like a stagnation flow. Therefore, the flow field is indeed a complicated 3D flow structure. Figure 7 compares the Nusselt number contours on the fin surface for the staggered and in-lined configurations. As expectedly, in-lined-lined tube array has a smaller Nusselt number than staggered tube array. It is also seen that for both arrays, in the neighborhood of the front face of tubes, the Nu is larger because the boundary layer is repeatedly interrupted by the tubes, whereas, at the rear of the tube, the Nu is lower because of the recirculation zone exists.

Figure 8 presents the variations of C_p and Nu around the tube surface from 1st to the 4th row at $X = 0.25$ for both staggered and in-lined arrays. The angle θ is measured from the front stagnation point of the tube. One can see that variations of the surface pressure profile for each row look similar, and the C_p value decreases in order from the 1st row to the 4th row. The magnitude of the pressure drop along the tube surface in a staggered array is higher than that in an in-lined array. For staggered array, the local Nusselt number for the 1st row has a maximum value at $\theta = 34°$, while for rows 2–4 the maximum Nu occurs at about $\theta = 70°$. For in-lined arrangement, the maximum Nu for the 1st row occurs at $\theta = 30°$ and the peak value is greater than that for the staggered arrangement. It is interesting to note that there are two local maximums for Nu for rows 2–4 because of the reattachment of the flow behind the 1st row, and these values are smaller than those for staggered arrangement. It should be noted that, only for the 1st row, the general trend of the variation of the Nusselt number vs θ is in agreement with those shown in Wung and Chen [7] for a 2D bare tube bundle.

The calculated averaged Nusselt numbers ($\overline{Nu}$) and dimensionless pressure drops ($\Delta\bar{P}$) at various Reynolds numbers ranging from 60 to 900 are shown in Figs. 9(a) and (b), respectively, for a heat exchanger with four-row deep, tube diameter 15.8 mm, tube center spacing 38 mm and fin pitch 8 fins in^{-1}. The solid and dashed lines represent the results for the staggered and in-lined arrays, respectively. It is seen that the average heat transfer coefficient of staggered arrangement is 15–27% higher than that of in-lined arrangement, while the pressure drop of staggered configuration is 20–25% higher than that of in-lined configuration. The numerical predictions of $\overline{Nu}$ for a 2D bare tube bundle obtained by Wung and Chen [7] are also shown in the figure for the comparisons between 2D and 3D models. It is observed that, for a staggered array, 2D model overestimates the average Nusselt number, while, for an in-lined array, the opposite trend is true.

In order to verify the validity of the present 3D

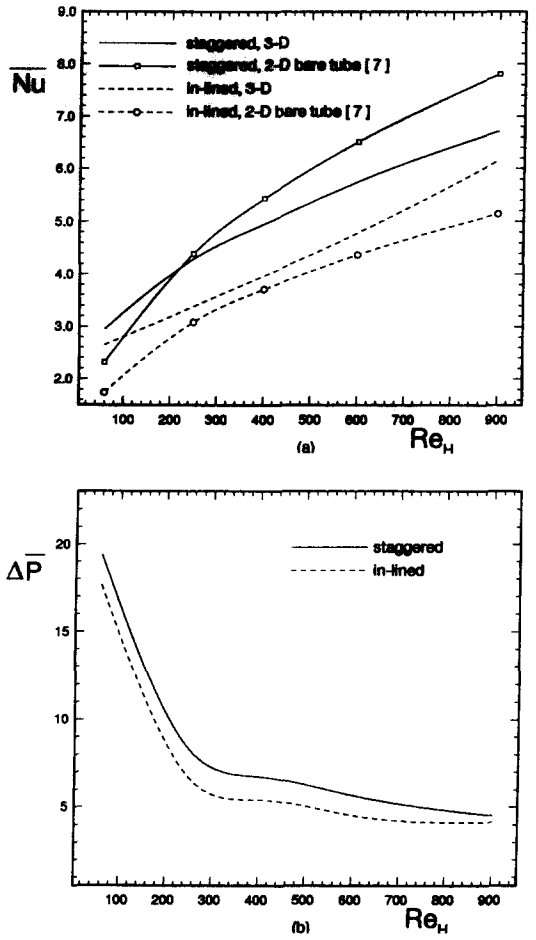

Fig. 9. The calculated $\overline{Nu}$ and $\Delta\bar{P}$ vs Re_H for staggered and in-lined arrangements.

laminar model and numerical prediction, the calculated and measured averaged heat transfer coefficient, $\bar{h}$ (W m^{-2} °C^{-1}), and pressure drop, $\Delta\bar{p}$(Pa), are presented in Figs. 10(a) and (b), respectively, for three four-row heat exchangers in staggered configuration with three different fin pitches (8, 10, 12 fins in^{-1}). Although the actual boundary condition for the surface heat transfer present in the experiment does not occur under constant wall temperature, the numerical results agree well with the experimental data. Both the numerical and experimental studies indicate that, for a given inlet frontal velocity, the average heat transfer coefficient and pressure drop increase as the fin pitches increase from 8 to 12 fins in^{-1}. In the industrial applications, the inlet frontal velocity for a plate-fin and tube heat exchanger is usually in the range of 2–4 m s^{-1} ($Re_H = 400$–800), therefore, the flow can be treated as laminar and the numerical method presented in this paper is accurate enough to predict the heat transfer and friction characteristics for such a heat exchanger.

The tube row effects on the averaged Nusselt number and pressure drop as a function of Re_H are illustrated in Figs. 11(a) and (b), respectively, for tube

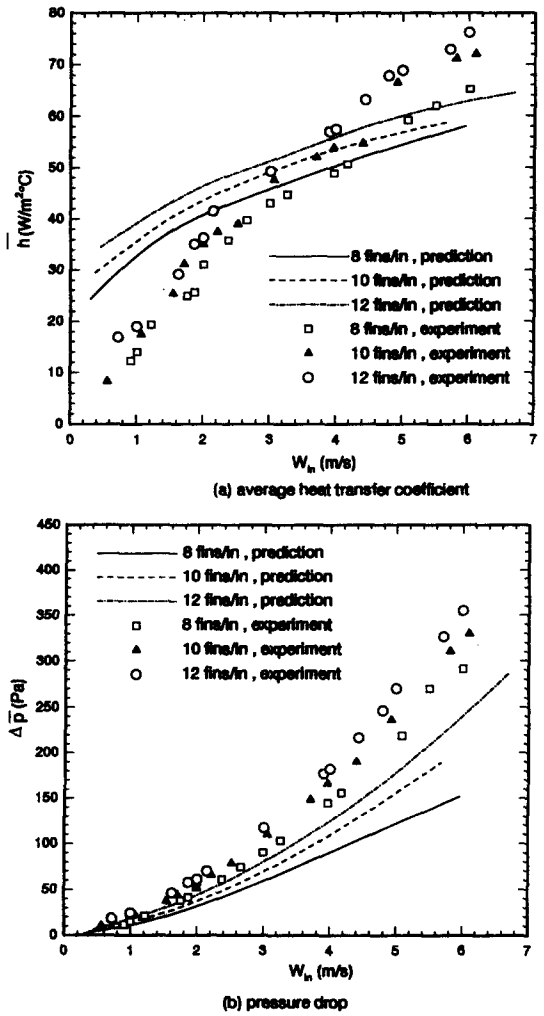

Fig. 10. The calculated and measured average heat transfer coefficient and pressure drop as a function of inlet frontal velocity.

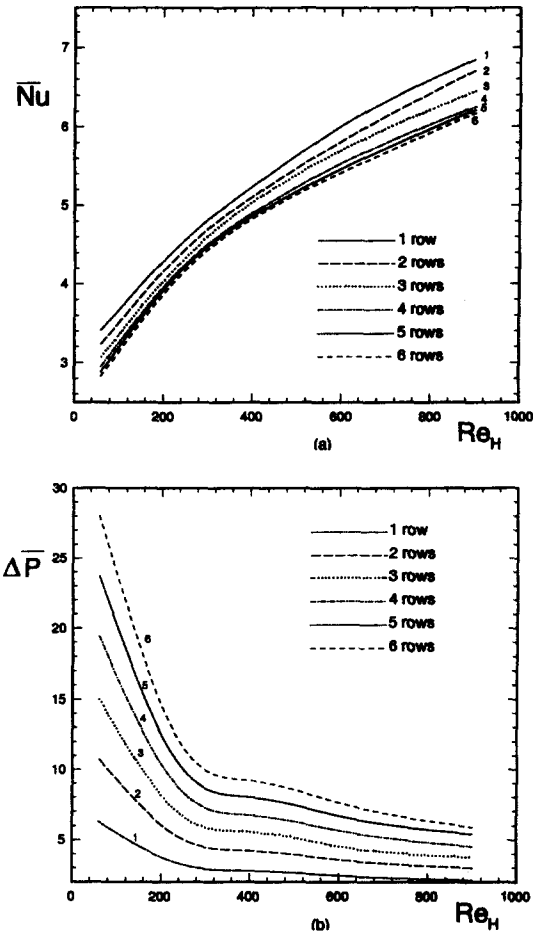

Fig. 11. The tube row effects on the $\overline{Nu}$ and $\Delta\bar{P}$ as a function of Re_H.

diameter 15.9 mm, fin pitch 8 fins in^{-1}, tube center spacing 38 mm and in staggered arrangement. It is seen that averaged Nusselt number is decreased as the number of tube rows is increased from 1 to 6. It is also found that the averaged heat transfer coefficient is nearly independent of the tube row number as the row numbers are greater than 4.

6. CONCLUSION

The computational and experimental studies of 3D laminar flow and heat transfer in a plate-fin and tube heat exchanger are presented. The numerical results demonstrate that the average heat transfer coefficient of staggered array is higher than that of in-lined array, while the pressure drop of staggered configuration is 20–25% higher than that of in-lined configuration. For in-lined array, the maximum value of Nusselt number for the 1st row around the tube surface is greater than that for the staggered array; there are two local maximums for rows 2–4, and these values are smaller than those for staggered array. For a staggered array, 2D model for a bare tube bundle overestimates the average Nusselt number, while, for an in-lined array, the opposite trend is true. It is also found that the number of tube row has a small effect on the average heat transfer coefficient as the row numbers are greater than 4. The numerical predictions agree well with experimental data.

Acknowledgements—The authors would like to thank Mr S. U. Lian for his help in conducting the experiment. Financial support for this work was provided by the National Science Council of Taiwan, R. O. C. under contract NSC84-2212-E006-004.

REFERENCES

1. A. Zukauskas, Heat transfer from tubes in crossflow, *Adv. Heat Transfer* **18**, 87–159 (1987).
2. A. Thom and C. J. Apelt, *Field Computation in Engineering and Physics*. Van Nostrand, London (1961).
3. R. F. Le Feuvre, Laminar and turbulent forced convection processes through in-line tube banks, HTS/74/5, Mechanical Engineering Department, Imperial College, London (1973).
4. B. E. Launder and T. H. Massey, The numerical prediction of viscous flow and heat transfer in tube banks, *ASME J. Heat Transfer* **100**, 565–571 (1978).

5. M. Fujii, T. Fujii and T. Nagata, A numerical analysis of laminar flow and heat transfer of air in an in-line tube bank, *Numer. Heat Transfer* **7**, 89–102 (1984).
6. T. S. Wung and C. J. Chen, Finite analytic solution of convective heat transfer for tube arrays in crossflow—I. Flow field analysis, *ASME J. Heat Transfer* **111**, 633–640 (1989).
7. T. S. Wung and C. J. Chen, Finite analytic solution of convective heat transfer for tube arrays in crossflow—II. Heat transfer analysis. *ASME J. Heat Transfer* **111**, 641–648 (1989).
8. D. Kundu, A. Haji-Sheikh and D. Y. S. Lou, Pressure and heat transfer in cross flow over cylinders between two parallel plates, *Numer. Heat Transfer, A*, **19**, 345–360 (1991).
9. D. Kundu, A. Haji-Shiekh and D. Y. S. Lou, Heat transfer predictions in cross flow over cylinders between two parallel plates, *Numer. Heat Transfer A*, **19**, 361–377 (1991).
10. D. Kundu, A. Haji-Shiekh and D. Y. S. Lou, Heat transfer in crossflow over cylinders between two parallel plates—An experimental study. In *Convective Heat Transfer in the Presence of an Obstructing Medium*, ASME winter meeting, 25–30 November, HTD-Vol.144, pp. 1–7, ASME. New York (1990).
11. F. E. M. Saboya and E. M. Sparrow, Local and average transfer coefficients for one-row plate fin and tube heat exchanger configurations. *ASME J. Heat Transfer* **96**, 265–272 (1974).
12. F. E. M. Saboya and E. M. Sparrow, Transfer characteristics of two row plate fin and tube heat exchanger configurations, *Int. J. Heat Mass Transfer* **19**, 41–49 (1976).
13. F. E. M. Saboya and E. M. Sparrow, Experiments on a three-row fin and tube heat exchanger, *J. Heat Transfer* **98**, 26–34 (1976).
14. D. G. Rich, The effect of fin spacing on the heat transfer and friction performance of multi-row plate fin-and-tube heat exchangers, *ASHRAE Trans.* **17**, 137–145 (1973).
15. D. G. Rich, The effect of the number of tube rows on the heat transfer performance of smooth plate and fin-and-tube heat exchangers, *ASHRAE Trans.* **81**, 307–317 (1975).
16. F. C. McQuiston, Correlation for heat, mass and momentum transport coefficients for plate-fin-tube heat transfer surfaces with staggered tube, *ASHRAE Trans.* **84**, 294–309 (1978).
17. D. L. Gray and R. L. Webb, Heat transfer and friction correlations for plate fin-and-tube heat exchangers having plain fins, *Proceedings of the Ninth International Heat Transfer Conference*, San Francisco (1986).
18. F. C. McQuiston and J. D. Parker, *Heating, Ventilating and Air Conditioning Analysis and Design*. John Wiley, New York (1994).
19. H. Yamashita, G. Kushida and R. Izumi, Fluid flow and heat transfer in a plate-fin and tube heat exchanger (Analysis of fluid flow around a square cylinder situated between parallel plates), *Bull. JSME*, **29**(254), 2562–2569 (1986).
20. H. Yamashita, G. Kushida and R. Izumi, Fluid flow and heat transfer in a plate-fin and tube heat exchanger (Analysis of fluid flow around a square cylinder situated between parallel plates), *Bull. JSME*, **29**(258), 4185–4191 (1986).
21. A. Bastini, M. Fiebig and N. K. Mitra, Numerical studies of a compact fin-tube heat exchanger, *Proceedings of the EUROTHERM Seminar* No. 18, *Design and Operation of Heat Exchangers*, 27 February–1 March, pp. 154–163. Hamburg, Germany (1991).
22. F. Zdravistch, C. A. J. Fletcher and M. Behnia, Laminar and turbulent heat transfer predictions in tube banks in cross flow, *Proceedings of the Int. Conference on Fluid and Thermal Energy Conversion*, pp. 29–34, 12–15 December, Kutta-Denpasar, Indonesia (1994).
23. S. V. Patankar, *Numerical Heat Transfer and Fluid Flows*. Hemisphere, Washington (1980).
24. ASHRAE Standard 41.2-1987, Standard Methods for Laboratory Air-Flow Measurement, American Society of Heating, Refrigerating and Air-Conditioning Engineers, Atlanta (1987).
25. W. M. Kays and A. L. London, *Compact Heat Exchangers* (3rd Edn). McGraw-Hill, New York (1984).
26. R. J. Moffat, Describing the uncertainties in experimental results, *Exp. Thermal Fluid Sci.* **1**, 3–17 (1988).